

Article

Protrusive Activity Guides Changes in Cell-Cell Tension during Epithelial Cell Scattering

Venkat Maruthamuthu¹ and Margaret L. Gardel^{1,2,*}¹Institute for Biophysical Dynamics and ²James Franck Institute and Department of Physics, University of Chicago, Chicago, Illinois

ABSTRACT Knowing how epithelial cells regulate cell-matrix and cell-cell adhesions is essential to understand key events in morphogenesis as well as pathological events such as metastasis. During epithelial cell scattering, epithelial cell islands rupture their cell-cell contacts and migrate away as single cells on the extracellular matrix (ECM) within hours of growth factor stimulation, even as adhesion molecules such as E-cadherin are present at the cell-cell contact. How the stability of cell-cell contacts is modulated to effect such morphological transitions is still unclear. Here, we report that in the absence of ECM, E-cadherin adhesions continue to sustain substantial cell-generated forces upon hepatocyte growth factor (HGF) stimulation, consistent with undiminished adhesion strength. In the presence of focal adhesions, constraints that preclude the spreading and movement of cells at free island edges also prevent HGF-mediated contact rupture. To explore the role of cell motion and cell-cell contact rupture, we examine the biophysical changes that occur during the scattering of cell pairs. We show that the direction of cell movement with respect to the cell-cell contact is correlated with changes in the average intercellular force as well as the initial direction of cell-cell contact rupture. Our results suggest an important role for protrusive activity resulting in cell displacement and force redistribution in guiding cell-cell contact rupture during scattering.

INTRODUCTION

The transition of cells from an epithelial phenotype with stable cell-cell contacts to a migratory mesenchymal phenotype with little to no cell-cell contacts is an important physiological process (1). Such epithelial-to-mesenchymal transitions (EMTs) play a crucial role during development as well as in pathological processes such as tumor progression (2). Even though much is known about the genetic program that underlies EMT (1), how cells physically orchestrate this transition is much less clear. Epithelial cell scattering is an *in vitro* model of EMT wherein islands of epithelial cells dissociate and migrate away as single cells in response to stimuli (3). Epithelial cell scattering of MDCK cells by hepatocyte growth factor (HGF, also known as scatter factor) stimulation occurs in the timescale of hours, does not involve the transcriptional changes of EMT, and is a convenient model system for studying how cells physically dissociate from one another.

It is generally thought that epithelial cell scattering occurs in two sequential stages: 1), dissociation of cell-cell contacts; and 2), migration of cells away from each other. Cells undergo dramatic morphological changes, including increased protrusive activity and a consequent increase in cell spread area within minutes of growth factor stimulation (3). The dissociation of cell-cell contacts is then thought to enable the cells to freely migrate away from each other (4). The dissociation of cell-cell contacts has been attributed to

decreased surface expression of E-cadherin (5) or downregulation of E-cadherin function by biochemical changes in cadherin or cadherin-associated proteins (6). However, the total level of E-cadherin (7) at the cell-cell contact has been reported to stay unchanged or only marginally decrease before cell scattering (8), thereby bringing into question whether HGF plays a direct role in the dissociation of cell-cell contacts.

Cadherin-mediated cell-cell junctions have been shown to support significant cell-generated actomyosin forces (9,10), with both an excess and lack of forces resulting in compromised junctional integrity (9). In an elegant paper by de Rooij and co-workers (11), it was suggested that increased forces at cell-cell contacts due to enhanced actomyosin contraction were responsible for the rupture of E-cadherin adhesions during cell scattering. On the other hand, it has been shown that the actin cytoskeleton disengages from cell-cell contacts prior to scattering, suggesting that cell-cell junctions are destabilized by decreased transmission of forces from the actin cytoskeleton (12). Whether the total level of forces at cell-cell contacts increases or decreases significantly to destabilize cell-cell junctions during cell scattering is thus an open question, as the level of forces at cell-cell contacts has not yet been quantitatively determined during this dynamic process.

In this report, we consider the morphological and physical processes that occur during HGF-induced scattering of MDCK epithelial cells. We first show that in the absence of focal adhesions, tension transmitted through E-cadherin-mediated adhesions does not decrease upon HGF

Submitted December 17, 2013, and accepted for publication June 18, 2014.

*Correspondence: gardel@uchicago.edu

Editor: Cecile Sykes.

© 2014 by the Biophysical Society
0006-3495/14/08/0555/9 \$2.00



<http://dx.doi.org/10.1016/j.bpj.2014.06.028>

stimulation. We then show that constraints on cell islands to prevent spreading and movement of cells at free edges impede cell-cell contact dissociation. In cell pairs, we show that the direction of cell movement with respect to the cell-cell contact preceding cell-cell contact dissociation is predictive of the direction of cell movement during cell-cell contact disruption. Finally, we find that the geometry of cell-cell contact dissociation is characterized by distinct changes in the average intercellular tension. Cell pairs that move orthogonal to the cell-cell contact dissociate abruptly, with an undiminished cell-cell tension preceding contact rupture. Cell pairs that move parallel to the cell-cell contact redistribute intracellular forces so that the tension at cell-cell contact decreases by ~50% before dissociation is observed. These data characterize the biophysical changes that occur during scattering of epithelial cells, and suggest that the redistribution of intracellular forces and adhesion strength play important roles in mediating changes in a highly context-dependent manner in response to HGF.

MATERIALS AND METHODS

Cell culture

MDCK cells (generously provided by Karl Matlin, University of Chicago) were grown under 5% CO₂ in low-glucose Dulbecco's modified Eagle's medium (DMEM; Gibco, Life Technologies, Grand Island, NY) with 1 g/l sodium bicarbonate (Thermo Fisher Scientific, Waltham, MA), penicillin-streptomycin (Life Technologies, Grand Island, NY), and 10% fetal bovine serum (FBS; HyClone, Logan, UT). Low-serum medium consisted of the same components, but with only 0.5% FBS. For cell plating on polyacrylamide (PAA) hydrogels, the cells were trypsinized and suspended as single cells. Then, ~10⁵ cells were plated in low-serum medium in a 60 mm dish containing the coverslip with the PAA gel ~20 h before experiments were conducted. For scattering experiments, HGF (Sigma-Aldrich, St. Louis, MO) at 5 ng/ml in low-serum medium was used for stimulation.

Protein purification

Purified recombinant protein consisting of the extracellular region of canine E-cadherin fused to an Fc portion (EcadFc) was expressed and purified as described previously (13). Briefly, HEK293 cells stably expressing and secreting the recombinant protein were cultured in high-glucose DMEM with 10% FBS. The cells were alternately cultured in this medium for 1 day followed by serum-free medium for 2 days, and this serum-free medium was collected and stored at 4°C. EcadFc was purified in one step using affinity chromatography with a protein A sepharose column (Pierce, Rockford, IL).

Immunofluorescence

Cells were fixed with 4% paraformaldehyde (Electron Microscopy Sciences, Hatfield, PA) in incubation buffer (PBS buffer that also contained 1.5% BSA and 0.5% Triton). Staining was performed using rabbit anti-paxillin (Santa Cruz Biotech, Dallas, TX) and anti-E-cadherin (BD Biosciences, San Jose, CA) antibodies followed by fluorophore-conjugated secondary antibodies and/or Alexa Fluor-conjugated phalloidin in incubation buffer.

Live-cell imaging

Wide-field imaging was performed with a Ti-E microscope (Nikon, Melville, NY), 20 × 0.75 multi-immersion Plan Fluor objective (Nikon, Melville, NY), and HQ2 cooled CCD camera (Roper Scientific, Tucson, AZ) controlled with Metamorph software (Molecular Devices, Sunnyvale, CA). For traction force measurements, imaging was performed with a multispectral spinning-disc confocal microscope that additionally included a CSU-X confocal scanner (Yokogawa, Newnan, GA) and a multiple-laser source (Applied Spectral Imaging, Carlsbad, CA). PAA gel coverslips were mounted in cell culture medium with 10 mM HEPES in a perfusion chamber and imaged at ~37°C. For traction force microscopy (TFM) experiments, trypsin (0.05%; Life Technologies) was perfused at the end of the experiment to detach cells and obtain bead reference images.

PAA hydrogel substrates

PAA gels attached to coverslips were prepared as described previously (14). The ratio of acrylamide to bis-acrylamide was 7.5%/0.1%, corresponding to a Young's modulus of 8.4 kPa. PAA gels used for TFM experiments contained 40 nm dark red beads to serve as deformation markers. Collagen I (BD Biosciences) was chemically cross-linked to the PAA gel surface by one of two methods. In the first method, the gel surface was activated by hydrazine hydrate (Sigma-Aldrich) overnight, followed by a 1 h incubation in 5% acetic acid (Thermo Fisher Scientific) and a 1 h wash in double distilled water (15). Oxidized collagen I was prepared by reacting 20 μg of collagen I with 40 μg of sodium metaperiodate in 1 ml sodium acetate buffer at pH 4.5. Oxidized collagen I was coupled to the activated gel surface by incubation for 1 h. In the second method, Sulfo-SANPAH (Pierce) was first coupled to the gel surface with a 12 mg/ml solution under 254 nm UV light at 1 J/cm² for 5 min (14). The gels were then washed and stored in PBS at 4°C. Gels used for TFM additionally contained 40 nm far-red beads (Life Technologies). To obtain E-cadherin-Fc-coated PAA surfaces, protein A (1 mg/ml) was first coupled to the gel surface using Sulfo-SANPAH as described above, followed by incubation with EcadFc (at ~10 μM) for 2 h at room temperature and a rinse in PBS.

Micropatterning on PAA hydrogels

Micropatterning on PAA hydrogels was performed as described by Tseng and co-workers (16). Quartz/chrome photomasks (Toppan, Round Rock, TX) with the desired micropatterns were cleaned with n-hexane. A ~30 μl drop of the 7.5%/0.1% acrylamide/bis-acrylamide mixture was placed on the chrome side of the photomask with the micropattern. A silanized coverslip was placed over the drop and polymerization was allowed to proceed for 45 min. The gel was then exposed through the photomask to deep UV light in a UV-Ozone cleaner (Jelight, Irvine, CA) for 2 min. The coverslip with the attached gel was then immersed in water and removed from the photomask. The gel was incubated with EDC (~10 mg/ml) and sulfo-NHS (~10 mg/ml; Pierce) in water for 25 min. This was followed by incubation with 0.1 mg/ml collagen I in 100 mM NaHCO₃ (pH 8.5) for 30 min at room temperature. After washing with water and PBS, ~10⁶ MDCK cells were plated onto the micropatterned gels in 60 mm culture dishes in low-serum culture media. The medium was changed after 16 h and experiments were then performed.

Cell-pair morphology measurements and rupture observations

Characterization of the morphological changes of epithelial cell pairs that occurred before scattering was performed as follows: From transmitted light images of cell pairs over time, cell boundaries for both cells were manually extracted. The centroid of each cell was computationally calculated from their binary masks using MATLAB (The MathWorks, Natick, MA) as a function of time. For any two successive time points (separated by 15–60 min),

the displacement of the centroid of each cell yielded the net direction in which the cell extended protrusions at that time. The difference between the centroid displacements of cell 1 and cell 2 yielded the direction in which cell 1 protruded away from cell 2 (see Fig. 4). The angle between the centroid relative displacement and the line joining the end points of the cell-cell contact yielded the relative polarization angle (θ_p). θ_p calculated for the two successive time points just before initiation of cell-cell contact rupture was a directional measure of the relative direction in which the cells of the cell pair were protruding away from each other. The initiation of cell-cell contact rupture was the time point at which brightfield imaging revealed that the cells either separated from each other orthogonal to the plane of cell-cell contact, forming a gap between the cells (see Figs. 4 A and S2 A in the Supporting Material), or abruptly decreased the extent of cell-cell contact by sliding past each other parallel to the plane of cell-cell contact, leading to cell separation (Figs. 4 B and S2 B). Out of 21 cell pairs, we observed 12 undergoing orthogonal rupture and nine undergoing parallel rupture. Since we monitored scattering over the timescale of ~ 5 h, our results are most relevant in the timescale of the first several hours after HGF stimulation.

Traction force measurements

High-resolution TFM was used to measure the traction forces exerted by the cells as described previously (10,17). Briefly, MDCK cells were plated on either collagen I- or EcadFc-coated PAA gels doped with submicron fluorescent beads. The images of the fluorescent beads at the top surface of the gel were recorded with the cells on the gel and after the cells were trypsinized off the gel. Using the images of the beads, displacement of the gel surface was calculated with the use of particle imaging velocimetry (PIV) software in MATLAB (The MathWorks, Natick, MA; available at <http://www.oceanwave.jp/software/mpiv/>). Traction forces were reconstructed from the displacements of the gel surface using regularized Fourier transform traction cytometry (18,19). For cell pairs, intercellular force was calculated as the imbalance in traction forces exerted by each cell in a cell pair as described previously (10).

RESULTS AND DISCUSSION

Epithelial cells transmit significant cell-generated forces to their microenvironment both before and after scattering

Epithelial cells adhere to a microenvironment that consists of both neighboring cells and the extracellular matrix (ECM). Epithelial cells have previously been shown to exert significant cell-generated forces on both cell-cell and cell-ECM interfaces (9,10,20). After HGF-stimulated scattering (Fig. 1 A), single epithelial cells adhere solely to the ECM. It has been suggested that HGF-stimulation may induce cell scattering by altering the traction forces transmitted by a cell to its microenvironment (11). To assess the contractile state of cells before and after scattering, we considered epithelial cell pairs, as they have a single, unique cell-cell interface. Using TFM (17) and the traction force imbalance method (9,10,20) on cell pairs plated on collagen-coated elastic PAA substrates, we found that cells exerted substantial tensile forces on their microenvironment (cell-ECM force per cell = 135 ± 65 nN and cell-cell force = 66 ± 24 nN, $n = 8$ cell pairs) in low-serum medium (Fig. 1, B–D). Importantly, the single cells that resulted from scattering continued to exert high tensile forces on their microenvironment (cell-ECM

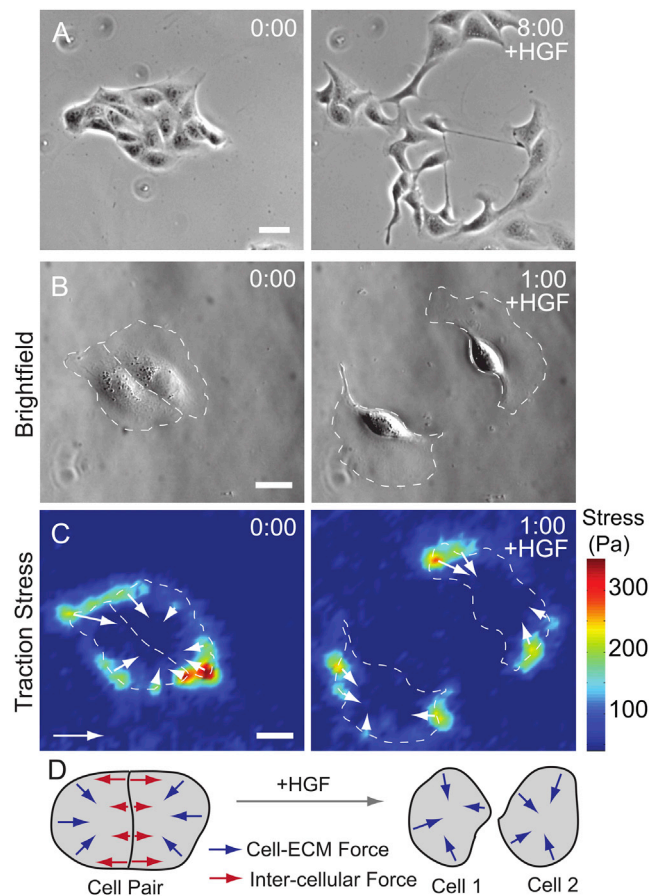


FIGURE 1 During scattering, epithelial cells transition from exerting force at both cell-cell and cell-ECM adhesions to exerting force solely at cell-ECM adhesions. (A) Island of MDCK epithelial cells on a collagen-coated PAA gel before and after scattering due to HGF stimulation. (B) Brightfield image of an MDCK cell pair on a collagen-coated PAA gel surface before and after scattering. (C) Heatmap of the magnitude of the traction stress exerted on the ECM by the cell pair in B before and after scattering. The color scale for the heatmap images is shown on the right. Local vector sums of prominent patches of traction forces are indicated as vectors (white arrows). Boundaries of the cells in B and C are indicated as dashed white lines. (D) Schematic depiction of intercellular and cell-ECM traction forces in a cell pair and in the resultant cells after scattering. Scale bar is $40 \mu\text{m}$ in A and $20 \mu\text{m}$ in B and C. Scale for traction vectors (white arrow) in C is 50 nN . Time in A–C is indicated in h:min. To see this figure in color, go online.

force = 142 ± 95 nN, $n = 16$ cells; Fig. 1, B–D). Thus, although HGF stimulation changes cell cohesion, it does not significantly alter the contractile state of the cells themselves. The cells generate substantial contractile tension both before and after scattering (Fig. 1, C and D).

Forces transmitted through E-cadherin adhesions do not decrease upon HGF stimulation in the absence of cell-ECM adhesion

Dissociation of cell-cell contacts is a key step that enables cells to freely migrate away from each other during cell scattering (4). In turn, cell-cell contact stability is dependent

on the strength of cell-cell adhesion. E-cadherin is the cardinal cell-cell adhesion molecule that mediates adhesion between epithelial cells, and adverse effects on E-cadherin adhesion are known to affect cell-cell contact stability (21). One hypothesis for the rupture of cell-cell contacts during epithelial cell scattering is that the adhesion strength of E-cadherin is reduced (22,23). Thus, we directly measured the effect of HGF on the tension transmitted through E-cadherin adhesions. Single MDCK cells were plated on biomimetic surfaces consisting of PAA hydrogels coated with the extracellular portion of E-cadherin (see Materials and Methods). Cells adhered to and spread on the E-cadherin-coated surfaces exclusively via E-cadherin-mediated adhesions (Fig. 2 A; Fig. S1, A and B), consistent with previous work (24,25). As shown in Fig. 2 A, cells generated significant traction forces on the E-cadherin-coated surface before stimulation with HGF (312 ± 108 nN). Five hours after HGF addition, the cells continued to exert large forces (321 ± 89 nN, $n = 13$). Cells that increased their spread area concomitantly increased their traction forces (Fig. S1, C–E). Thus, the cell-generated tension transmitted (via E-cadherin adhesions) per unit cell area remained the same 5 h after HGF stimulation (94 ± 18 pN/ μm^2) as compared with before HGF stimulation (100 ± 26 pN/ μm^2) as averaged for $n = 13$ individual cells (Fig. 2 B, $p = 0.4$). Additionally, we also confirmed that E-cadherin adhesions were present even after overnight stimulation with HGF (Fig. S1 B), consistent with a previous report (11). Thus, in the absence of focal adhesions, E-cadherin adhesions not only persist upon HGF stimulation but also withstand substantial forces. This suggests that cells require simultaneous interaction with the ECM to adversely affect their E-cadherin adhesions upon HGF stimulation.

Continuous formation of new peripheral protrusions and adhesion to surrounding ECM are required for cell-cell contact rupture during scattering

The initial response to HGF stimulation is the extensive formation of protrusions and increased spreading (26,27).

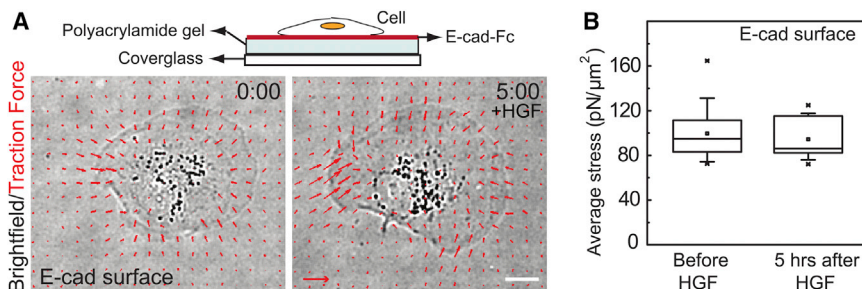


FIGURE 2 E-cadherin adhesions support large cell-generated forces after HGF stimulation. (A) A single MDCK cell adhering to an EcadFc-coated PAA gel was stimulated with HGF. A brightfield image of the MDCK cell and the traction stress (red arrows) exerted by the cell on the EcadFc-coated surface before and 5 h after HGF stimulation is shown, and a schematic of the experiment is shown above. (B) Box-and-whisker plot of the average stress exerted by MDCK cells through E-cadherin adhesions before and 5 h after HGF stimulation ($n = 13$ cells). The box-and-whisker plot indicates median (middle line), mean (small square), 25% and 75% (box lower and upper bounds), and 5% and 95% (whiskers) values. In A, the scale for traction stress vectors (red arrow) is 250 Pa, distance (white bar) is 10 μm , and time is indicated in h:min. See also Fig. S1. To see this figure in color, go online.

We therefore hypothesized that preventing cell spreading would impair HGF-mediated cell-cell contact dissolution. To accomplish this, we seeded epithelial cell islands on micropatterned regions of collagen surrounded by a nonadhesive surface (Fig. 3 A). When the cell island initially occupied nearly all of the available ECM area, stimulation with HGF did not lead to rupture of cell-cell contacts (Fig. 3 A). Newly formed peripheral protrusions rapidly adhered to any residual ECM, but any further adhesion was not possible due to confinement by the micropattern. No transient cell-cell contact rupture events were observed during or after expansion of the cell island to occupy the remaining residual ECM area. E-cadherin remained at cell-cell contacts and paxillin was localized to the island periphery even after overnight stimulation with HGF (Fig. 3 B). By contrast, when the cell island initially occupied only a fraction of the available ECM area, cell-cell contact rupture events were observed after HGF stimulation (Fig. 3 C). Stimulation with HGF led to new peripheral protrusions into the available ECM and rupture of cell-cell contacts as the cells migrated away from each other. Although in principle it is possible that cells may signal to their cell-cell contacts differently based on confinement or the surrounding free space, the most direct conclusion our results lead to is that morphological changes involved in de novo peripheral protrusion and adhesion at the free edges of cell islands into cell-free regions of ECM are required for cell-cell contact rupture.

Protrusive activity is correlated with the mode of cell-cell contact rupture

To assess the physical changes that take place during epithelial cell scattering, we measured the morphological and force changes that occurred during scattering of MDCK cell pairs (see Materials and Methods). When stimulated with HGF, we observed that the cells typically ruptured their cell-cell contact in two distinct geometries. In some cell pairs, the cells separated from each other perpendicular (orthogonal) to the plane of cell-cell contact

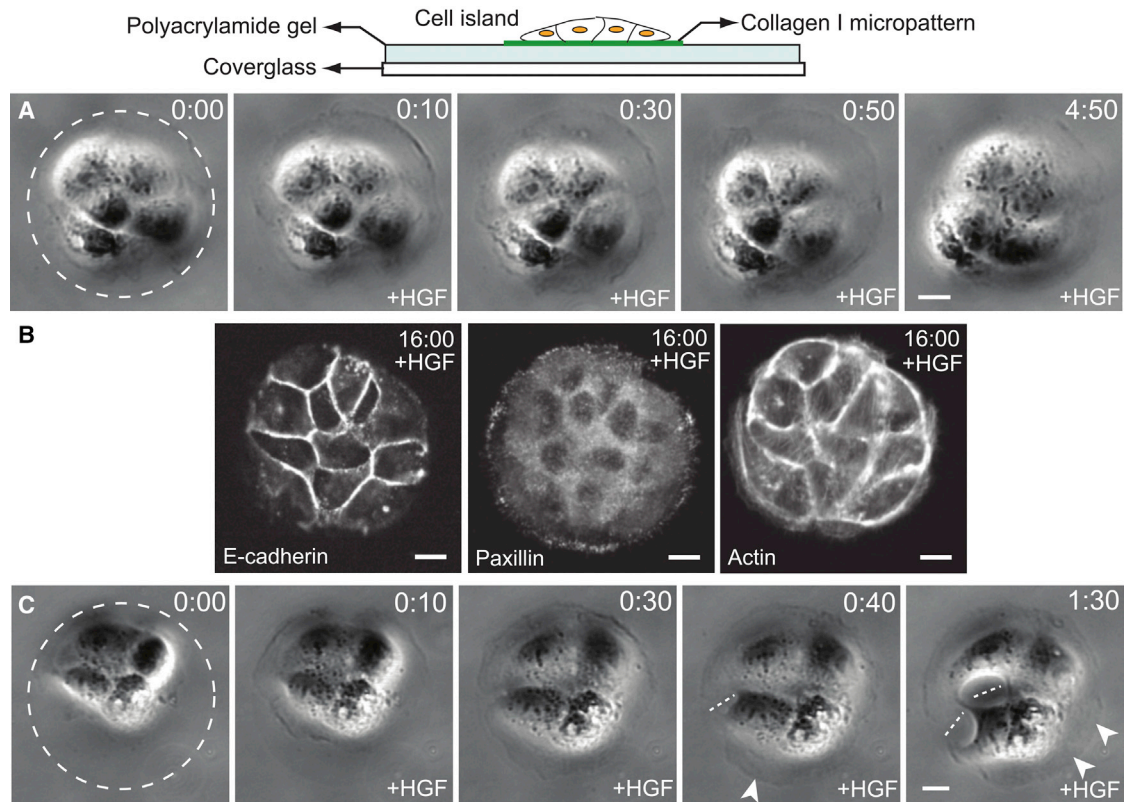


FIGURE 3 Continuous cell protrusion and adhesion to surrounding ECM is required for cell scattering. (A) Time lapse of brightfield images of an MDCK cell island adhering to and nearly completely occupying a circular collagen micropattern (*dotted circle*) stimulated with HGF after time 0. The sample setup is depicted above. (B) An MDCK cell island on a circular micropatterned collagen region was stimulated overnight with HGF and stained for E-cadherin, paxillin, and actin. Note the prominent localization of E-cadherin at cell-cell contacts. (C) Time lapse of brightfield images of a cell island occupying only approximately half of the available ECM area (outlined by *dotted circle*) and responding to HGF stimulation over several hours. Arrowheads in A and C indicate the location of new protrusions that bind to the ECM as cell-cell contact rupture (*dotted white line*) occurs. In A–C, the scale bar is 10 μm and time is indicated in h:min. To see this figure in color, go online.

(Figs. 4 A and S2 A), whereas in other cell pairs the cells ruptured their cell-cell contact by sliding past each other parallel to the plane of cell-cell contact (Figs. 4 B and S2 B). We then asked whether the nature of the morphological changes of the cells just before the initiation of cell-cell contact rupture determined the mode of contact rupture.

We characterized the cell movements by observing the evolution of the position of the centroids of the two cells (Fig. 4, A–C). We defined the relative protrusion angle θ_p as the angle between the relative cell displacement vector and the cell-cell contact line (Fig. 4 C). We found that the relative protrusion angle before cell-cell contact rupture was correlated with the type of contact rupture (Fig. 4 D). Orthogonal rupture events had a significantly higher relative protrusion angle than parallel rupture events (Figs. 4 D and S2 C). This means that the protrusive activity prior to cell-cell contact rupture was correlated with the manner in which contacts came apart. Our results are consistent with previous studies that suggested that spatially regulated increases in protrusive activity and contractility underlie epithelial cell scattering (28,29).

Protrusive activity is correlated with distinct intercellular mechanics

To identify differences in cell mechanics during the different modes of cell scattering, we quantified the evolution of total forces exerted at focal and cell-cell adhesions. In orthogonal rupture, the traction force distribution changes little after HGF addition up until the cell-cell contact ruptures (Fig. 5, A and C; same cell pair as in Fig. 4 A). In these cases, traction forces are localized around the periphery of the cell pair and the intercellular force remains high, without increasing or decreasing significantly from the pre-HGF value until cell-cell contact rupture occurs. After rupture occurs (indicated by asterisk), the intercellular tension decreases rapidly (Fig. 5 C). In contrast, in parallel rupture events, the traction forces redistribute upon HGF addition such that they slowly become internally balanced within each cell (Fig. 5, B and D; same cell pair as in Fig. 4 B). This redistribution of forces results in a diminished tension of, on average, $\sim 50\%$ at the cell-cell contact before rupture occurs (Fig. 5 E). Here, the ratio of the average intercellular forces to the total cell-ECM forces

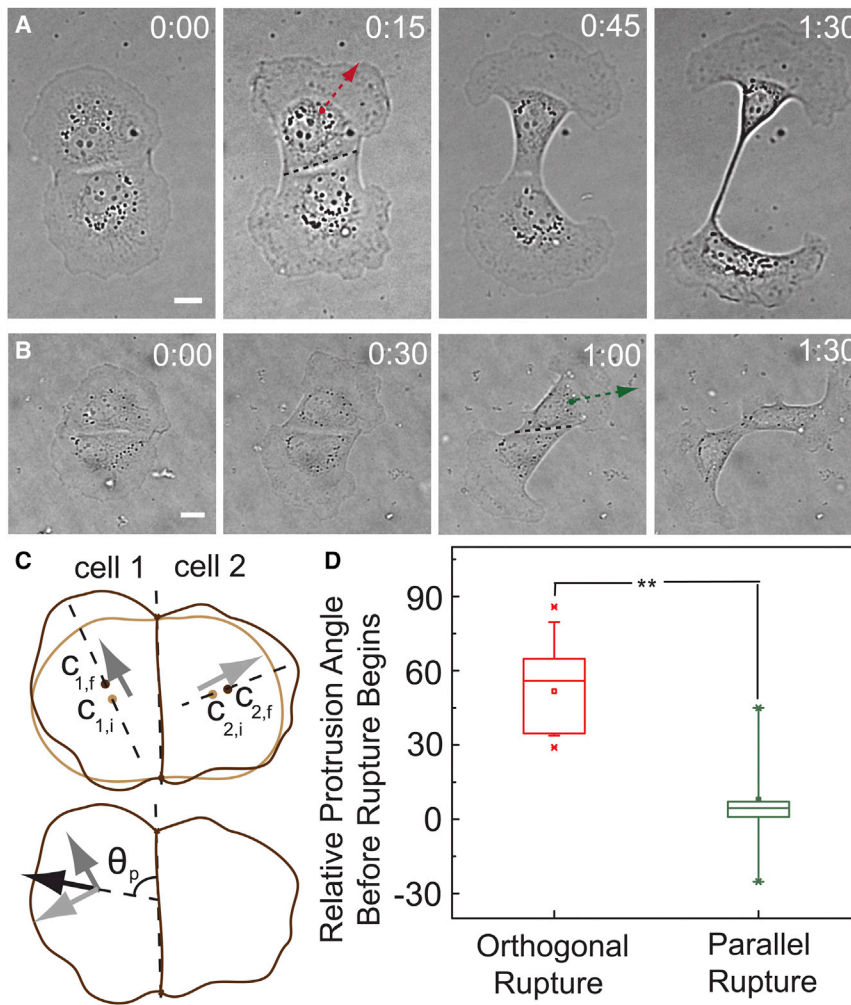


FIGURE 4 Direction of protrusions is coupled to the mode of cell-cell contact rupture initiation upon HGF stimulation. (A) Brightfield image of an MDCK cell pair plated on collagen scattering by orthogonal rupture of its cell-cell contact upon HGF stimulation. The dotted red arrow indicates the net direction of cell movement before contact rupture begins. The dotted black line indicates the cell-cell contact. (B) Brightfield image of an MDCK cell pair plated on collagen scattering by parallel rupture of its cell-cell contact upon HGF stimulation. The dotted green arrow indicates the net direction of movement before rupture begins. The dotted black line indicates the cell-cell contact. (C) Schematic depiction of the calculation of the relative protrusion angle (θ_p). In the upper image, the displacement vectors of the centroid of cell 1 ($C_{1,i}$ to $C_{1,f}$) and the centroid of cell 2 ($C_{2,i}$ to $C_{2,f}$) between the two successive time points (i and f) just before contact rupture initiates are indicated by dark and light gray arrows, respectively. The difference between these two vectors (shown as a *black arrow* in the lower image) is the relative direction of protrusion between the cells. The angle between this relative direction of protrusion and the cell-cell contact line (*dashed line*) is the relative protrusion angle (θ_p). Cell boundaries for the two consecutive time points just before contact rupture initiates are shown in light and dark brown, respectively. (D) Box-and-whisker plot showing the relative protrusion angle before cell-cell contact rupture occurs, for the two modes of contact rupture ($n = 12$ and 9 cell pairs undergoing orthogonal and parallel rupture, respectively). The box-and-whisker plot indicates median (*middle line*), mean (*small square*), 25% and 75% (*box lower and upper bounds*), and minimum and maximum (*whiskers*) values. In A and B, the scale bar is $10 \mu\text{m}$ and time is indicated in h:min. See also Fig. S2. To see this figure in color, go online.

decreases by a factor of 3 in the time leading up to rupture (Fig. S3 B).

We classified all of the ruptures we observed as either orthogonal or parallel based on the direction of cell motion at the time of contact rupture (Fig. S2). In orthogonal rupture, cells move away from each other perpendicular to the cell-cell contact and little change in the tension at the cell-cell contact occurs at times before rupture. In parallel rupture, the cells move away from each other parallel to the cell-cell contact and the average force sustained at the contact decreases gradually. To determine whether cell-cell contact rupture occurred along a continuum between these two conditions, we measured the changes in average cell-cell tension immediately preceding rupture as a function of the relative protrusion angle. We observed a correlation between these two quantities (Fig. 5 F), with smaller protrusion angles coinciding with larger decreases in average intercellular force preceding rupture. These results indicate that our finding could be applied more generally

to cell-cell contact dissociation, which should exist along a continuum from orthogonal to parallel rupture.

How do physical changes promote cell-cell contact dissolution during scattering?

Our data provide new (to our knowledge) biophysical insights into epithelial cell scattering. We find that in the absence of focal adhesions and available ECM to support increased spreading and morphological changes of the free edges, HGF does not induce the dissociation of cell-cell contacts. The tension exerted at the cell-cell adhesions remains high and the contact remains intact over long periods of time. This indicates that HGF does not promote weakening of the cell-cell contact directly, but does so through cross talk with cell-migratory modules involving the actin cytoskeleton and focal adhesions. Such cross talk has been suggested previously, with the standing hypothesis being that HGF induces increased tension at focal adhesions and cell-cell adhesions,

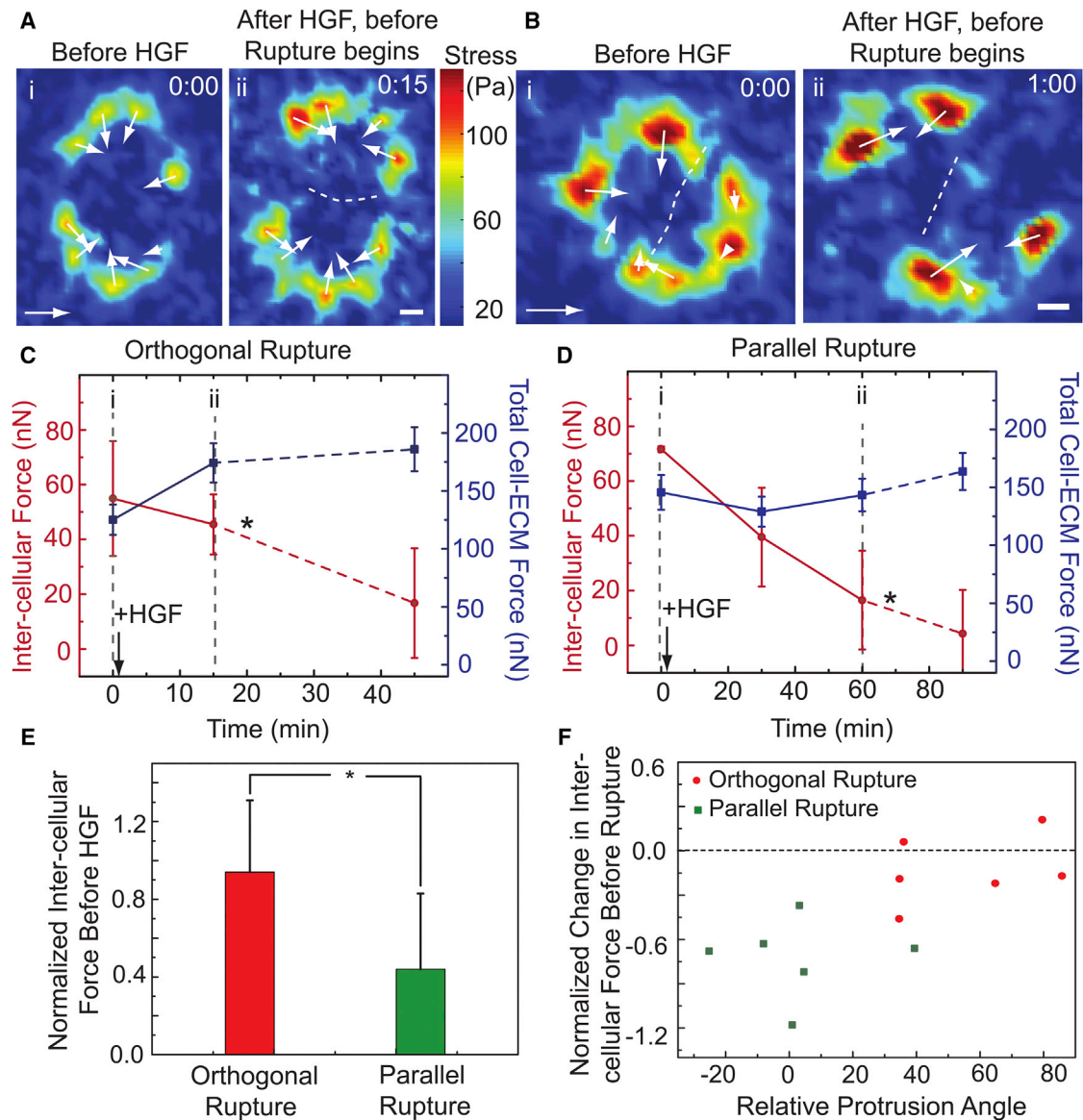


FIGURE 5 Cell pairs initiate orthogonal or parallel cell-cell contact rupture at distinct states of cell-cell tension. (*A* and *B*) Heatmap images of traction forces exerted by the MDCK cell pair shown in Fig. 4 *A* plated on collagen-coated gel (*i*) before HGF stimulation and (*ii*) just before initiation of orthogonal cell-cell contact rupture. (*B*) Heatmaps of traction forces exerted by the MDCK cell pair (shown in Fig. 4 *B*) (*i*) before HGF stimulation and (*ii*) just before initiation of parallel cell-cell contact rupture. Local vector sums of prominent patches of traction forces in *A* and *B* are indicated as vectors (white arrows) and time is in h:min. The scale bar for vectors is 40 nN in *A* and 65 nN in *B*. The scale bar for distance in *A* and *B* is 10 μ m. (*C*) Plot of the intercellular force and the total cell-ECM traction force as a function of time after HGF stimulation for the cell pair in *A*; * denotes rupture initiation. (*D*) Plot of the intercellular force (solid circles) and the total cell-ECM traction force (solid squares) as a function of time after HGF stimulation for the cell pair in *B*; * denotes rupture initiation. Time points for HGF stimulation (+HGF) and for those corresponding to the images in *A* and *B* are indicated as (*i*) and (*ii*), respectively, in the plots in *C* and *D*. (*E*) Bar graph of the intercellular force just before initiation of cell-cell contact rupture relative to the initial intercellular force before HGF stimulation for the two modes of rupture. (*F*) Plot of the change in intercellular force between the two time points just before rupture as a function of the relative protrusion angle for several cell pairs; $n = 12$ cell pairs in *E* and *F*. Error bars represent \pm SD. See also Fig. S3. To see this figure in color, go online.

resulting in preferential disruption of cell-cell contacts (11). However, our results are inconsistent with this model, as we find that tension at cell-cell contacts stays constant or decreases after HGF addition.

Our results lead to a conundrum: how do focal adhesion dynamics and morphological changes result in cell-cell con-

tact dissolution if the cell-cell contact is not being disrupted by overall increased tension or diminished adhesion strength? One way to reconcile these observations is to consider possible changes in the distribution of cell-cell adhesions and local cell-cell tension resulting from HGF-induced morphological changes. The actin cytoskeleton

reorganizes considerably during epithelial cell scattering (11,12,22,30,31). In unstimulated MDCK cell pairs, F-actin bundles coinciding with dense E-cadherin plaques are found mainly at the edges of cell-cell contacts (10,32,33). Accordingly, immunofluorescence imaging in cell pairs after HGF addition revealed differently organized F-actin and E-cadherin at the cell-cell contact in cell pairs with morphologies consistent with orthogonal (Fig. S4 A) or parallel (Fig. S4 B) rupture. Importantly, in both cases, prominent F-actin bundles were attached to regions within the cell-cell contact, and E-cadherin plaques became distended in an orthogonal or parallel manner, respectively. This is consistent with previous findings (11,34). We speculate that these changes in F-actin organization may coincide with rearrangements in local forces at the cell-cell contact. In the case of orthogonal rupture, we speculate that changes in F-actin along the contact lead to local force maxima that exceed the adhesion strength, even though the total intercellular force is unchanged. In the parallel case, the redistribution of forces to increased local parallel tension at the cell-cell contact and concomitant decrease in the measured intercellular force may promote parallel cell-cell contact disassembly. Future experiments to test this model will be necessary.

Even though all ruptures observed by phase imaging of cells were classified as either orthogonal or parallel based on the direction of cell motion compared with the cell-cell contact boundary (*red and green data points in Fig. 5 F*), the relative in-plane polarization of the cells (*x axis in Fig. 5 F*) exhibited a continuum. Clear cases on either end of this continuum are shown in Fig. 6, where the cells are polarized either orthogonal or parallel to the cell-cell contact. An intermediate case that is likely to be in the middle of this continuum, where one cell is (in-plane) polarized away from and orthogonal to the cell-cell contact whereas

the other is polarized away from but parallel to the cell-cell contact, is depicted in Fig. S5. In cell islands, we expect rupture events to be heterogeneous and include features of both kinds of rupture, especially as initiated rupture events proceed to completion. Notably, we found that E-cadherin puncta and F-actin bundles could be aligned either orthogonal to or parallel to the cell-cell contacts of cell islands beginning to undergo scattering (Fig. S4 C). Small epithelial cell islands have a predominantly peripheral localization of traction forces (35) and measurements in larger epithelial monolayers (36) have shown cooperative normal forces over ≥ 10 cell diameters. Thus, in larger islands, we expect that the peripheral protrusive activity may be related to the junctional forces and rupture events at longer distances.

In conclusion, we find that HGF stimulation does not decrease E-cadherin adhesion strength and that morphological changes in a free cell edge are required for rupture of cell-cell contacts. The directional nature of the protrusions on the ECM is correlated with the level of forces at the cell-cell interface and how the contact rupture is initiated. Our findings provide a physical picture of how changes in cell morphology affect cell-cell contact stability and suggest how mechanical cross talk between cell-cell and cell-ECM adhesions (37) can influence supracellular organization. Knowing how physical factors such as cell shape and cell-microenvironment forces are integrated with biochemical cues to specify multicellular architecture (38,39) will be essential to gain a more complete understanding of tissue structure and function.

SUPPORTING MATERIAL

Five figures are available at [http://www.biophysj.org/biophysj/supplemental/S0006-3495\(14\)00671-7](http://www.biophysj.org/biophysj/supplemental/S0006-3495(14)00671-7).

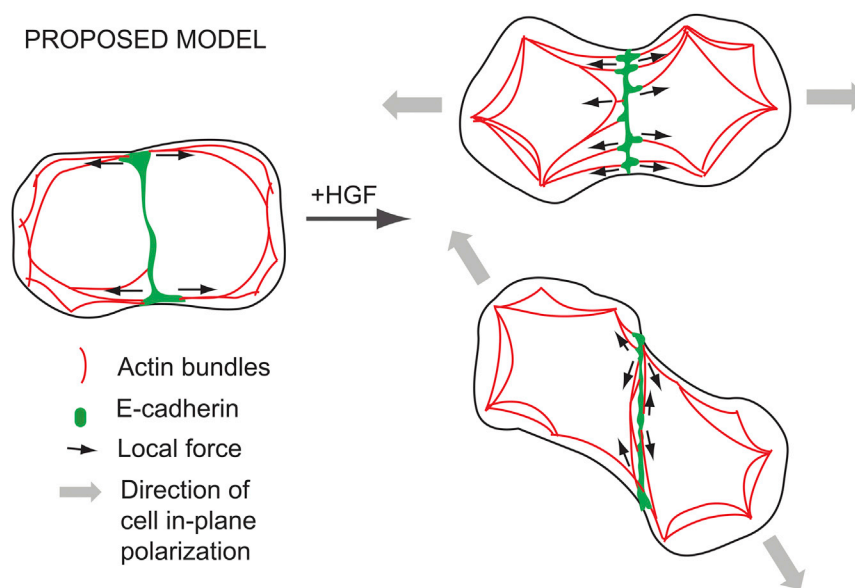


FIGURE 6 Proposed model for cell-cell contact rupture initiation, consistent with experimental data. Cell pairs before HGF stimulation (*left*) show prominent F-actin (*red*) organization as well as intercellular force localization at the edges of the cell-cell contact (10). In cell pairs about to undergo orthogonal rupture (*top right*), the cells protrude away from and orthogonal to the cell-cell contact (*broad gray arrows*) and cellular F-actin (*red*) reorganizes such that F-actin bundles terminate orthogonal to the cell-cell contact at several sites within the contact. We propose that this corresponds to intercellular force that is redistributed within the contact at local sites as depicted. In cell pairs about to undergo parallel rupture (*bottom right*), the cells protrude away from each other parallel to the cell-cell contact (*broad gray arrows*), and cellular F-actin (*red*) reorganizes such that several F-actin bundles terminate at the cell-cell contact in a parallel manner. We propose that this corresponds to significant intrajunctional tension that acts parallel to the cell-cell contact to enable rupture. See also Figs. S4 and S5. To see this figure in color, go online.

We thank James Nelson, Karl Matlin, Nicolas Borghi, and Kathy Siemers for generously providing reagents. We thank Ulrich Schwarz and Benedikt Sabass for the code to calculate traction stresses.

M.L.G. acknowledges support from a Burroughs Wellcome Career Award and Packard Fellowship. V.M. was supported in part by an American Heart Association Midwest Affiliate Postdoctoral Fellowship.

REFERENCES

- Thiery, J. P. 2003. Epithelial-mesenchymal transitions in development and pathologies. *Curr. Opin. Cell Biol.* 15:740–746.
- Thiery, J. P. 2002. Epithelial-mesenchymal transitions in tumour progression. *Nat. Rev. Cancer.* 2:442–454.
- Stoker, M., E. Gherardi, ..., J. Gray. 1987. Scatter factor is a fibroblast-derived modulator of epithelial cell mobility. *Nature.* 327:239–242.
- Clark, P. 1994. Modulation of scatter factor/hepatocyte growth factor activity by cell-substratum adhesion. *J. Cell Sci.* 107:1265–1275.
- Miura, H., K. Nishimura, ..., A. Okuyama. 2001. Effects of hepatocyte growth factor on E-cadherin-mediated cell-cell adhesion in DU145 prostate cancer cells. *Urology.* 58:1064–1069.
- Shibamoto, S., M. Hayakawa, ..., F. Ito. 1994. Tyrosine phosphorylation of beta-catenin and plakoglobin enhanced by hepatocyte growth factor and epidermal growth factor in human carcinoma cells. *Cell Adhes. Commun.* 1:295–305.
- Weidner, K. M., J. Behrens, ..., W. Birchmeier. 1990. Scatter factor: molecular characteristics and effect on the invasiveness of epithelial cells. *J. Cell Biol.* 111:2097–2108.
- Loerke, D., Q. le Duc, ..., J. de Rooij. 2012. Quantitative imaging of epithelial cell scattering identifies specific inhibitors of cell motility and cell-cell dissociation. *Sci. Signal.* 5:rs5.
- Liu, Z., J. L. Tan, ..., C. S. Chen. 2010. Mechanical tugging force regulates the size of cell-cell junctions. *Proc. Natl. Acad. Sci. USA.* 107:9944–9949.
- Maruthamuthu, V., B. Sabass, ..., M. L. Gardel. 2011. Cell-ECM traction force modulates endogenous tension at cell-cell contacts. *Proc. Natl. Acad. Sci. USA.* 108:4708–4713.
- de Rooij, J., A. Kerstens, ..., C. M. Waterman-Storer. 2005. Integrin-dependent actomyosin contraction regulates epithelial cell scattering. *J. Cell Biol.* 171:153–164.
- Mangold, S., S. K. Wu, ..., A. S. Yap. 2011. Hepatocyte growth factor acutely perturbs actin filament anchorage at the epithelial zonula adherens. *Curr. Biol.* 21:503–507.
- Drees, F., A. Reilein, and W. J. Nelson. 2005. Cell-adhesion assays: fabrication of an E-cadherin substratum and isolation of lateral and basal membrane patches. *Methods Mol. Biol.* 294:303–320.
- Yeung, T., P. C. Georges, ..., P. A. Janmey. 2005. Effects of substrate stiffness on cell morphology, cytoskeletal structure, and adhesion. *Cell Motil. Cytoskeleton.* 60:24–34.
- Damljanović, V., B. C. Lagerholm, and K. Jacobson. 2005. Bulk and micropatterned conjugation of extracellular matrix proteins to characterized polyacrylamide substrates for cell mechanotransduction assays. *Biotechniques.* 39:847–851.
- Tseng, Q., I. Wang, ..., M. Balland. 2011. A new micropatterning method of soft substrates reveals that different tumorigenic signals can promote or reduce cell contraction levels. *Lab Chip.* 11:2231–2240.
- Sabass, B., M. L. Gardel, ..., U. S. Schwarz. 2008. High resolution traction force microscopy based on experimental and computational advances. *Biophys. J.* 94:207–220.
- Butler, J. P., I. M. Tolić-Nørrellykke, ..., J. J. Fredberg. 2002. Traction fields, moments, and strain energy that cells exert on their surroundings. *Am. J. Physiol. Cell Physiol.* 282:C595–C605.
- Schwarz, U. S., N. Q. Balaban, ..., S. A. Safran. 2002. Calculation of forces at focal adhesions from elastic substrate data: the effect of localized force and the need for regularization. *Biophys. J.* 83:1380–1394.
- Treat, X., M. R. Wasserman, ..., J. J. Fredberg. 2009. Physical forces during collective cell migration. *Nat. Phys.* 5:426–430.
- Cavey, M., and T. Lecuit. 2009. Molecular bases of cell-cell junctions stability and dynamics. *Cold Spring Harb. Perspect. Biol.* 1:a002998.
- Balkovetz, D. F., and V. Sambandam. 1999. Dynamics of E-cadherin and gamma-catenin complexes during dedifferentiation of polarized MDCK cells. *Kidney Int.* 56:910–921.
- Fukata, M., M. Nakagawa, ..., K. Kaibuchi. 2001. Involvement of IQGAP1, an effector of Rac1 and Cdc42 GTPases, in cell-cell dissociation during cell scattering. *Mol. Cell. Biol.* 21:2165–2183.
- Kovacs, E. M., M. Goodwin, ..., A. S. Yap. 2002. Cadherin-directed actin assembly: E-cadherin physically associates with the Arp2/3 complex to direct actin assembly in nascent adhesive contacts. *Curr. Biol.* 12:379–382.
- Ladoux, B., E. Anon, ..., R.-M. Mège. 2010. Strength dependence of cadherin-mediated adhesions. *Biophys. J.* 98:534–542.
- Gimond, C., A. van Der Flier, ..., A. Sonnenberg. 1999. Induction of cell scattering by expression of beta1 integrins in beta1-deficient epithelial cells requires activation of members of the rho family of GTPases and downregulation of cadherin and catenin function. *J. Cell Biol.* 147:1325–1340.
- Ridley, A. J., P. M. Comoglio, and A. Hall. 1995. Regulation of scatter factor/hepatocyte growth factor responses by Ras, Rac, and Rho in MDCK cells. *Mol. Cell. Biol.* 15:1110–1122.
- Avizienyte, E., V. J. Fincham, ..., M. C. Frame. 2004. Src SH3/2 domain-mediated peripheral accumulation of Src and phospho-myosin is linked to deregulation of E-cadherin and the epithelial-mesenchymal transition. *Mol. Biol. Cell.* 15:2794–2803.
- Sander, E. E., S. van Delft, ..., J. G. Collard. 1998. Matrix-dependent Tiam1/Rac signaling in epithelial cells promotes either cell-cell adhesion or cell migration and is regulated by phosphatidylinositol 3-kinase. *J. Cell Biol.* 143:1385–1398.
- Rosen, E. M., L. Meromsky, ..., E. Setter. 1990. Studies on the mechanism of scatter factor. Effects of agents that modulate intracellular signal transduction, macromolecule synthesis and cytoskeleton assembly. *J. Cell Sci.* 96:639–649.
- Dowrick, P. G., A. R. Prescott, and R. M. Warn. 1991. Scatter factor affects major changes in the cytoskeletal organization of epithelial cells. *Cytokine.* 3:299–310.
- Zhang, J., M. Betson, ..., V. M. M. Braga. 2005. Actin at cell-cell junctions is composed of two dynamic and functional populations. *J. Cell Sci.* 118:5549–5562.
- Huveneers, S., and J. de Rooij. 2013. Mechanosensitive systems at the cadherin-F-actin interface. *J. Cell Sci.* 126:403–413.
- Huveneers, S., J. Oldenburg, ..., J. de Rooij. 2012. Vinculin associates with endothelial VE-cadherin junctions to control force-dependent remodeling. *J. Cell Biol.* 196:641–652.
- Mertz, A. F., S. Banerjee, ..., E. R. Dufresne. 2012. Scaling of traction forces with the size of cohesive cell colonies. *Phys. Rev. Lett.* 108:198101.
- Tambe, D. T., C. C. Hardin, ..., X. Trepat. 2011. Collective cell guidance by cooperative intercellular forces. *Nat. Mater.* 10:469–475.
- Weber, G. F., M. A. Bjerke, and D. W. DeSimone. 2011. Integrins and cadherins join forces to form adhesive networks. *J. Cell Sci.* 124:1183–1193.
- Fernandez-Gonzalez, R., and J. A. Zallen. 2009. Cell mechanics and feedback regulation of actomyosin networks. *Sci. Signal.* 2:pe78.
- Li, D., J. Zhou, ..., F. Wang. 2010. Integrated biochemical and mechanical signals regulate multifaceted human embryonic stem cell functions. *J. Cell Biol.* 191:631–644.